RSC Advances

BSA binding to silica capped gold nanostructures: effect of surface cap and conjugation design on nanostructure–BSA interface†

Shoba Narayan,*[a] Ashwini Rajagopalan,[a] Jannampalli Shruthi Reddy[a] and Anju Chadha*[ab]

This paper presents a detailed and systematic study of amine functionalization of silica coating of gold nanostructures and the electrostatic and covalent binding of the prepared silica capped gold nanostructures to BSA. The involvement of a Tryptophan residue in the hydrophobic pocket of BSA and its interaction with nanostructures was established. Fluorescence studies of tryptophan residues of the protein molecules after conjugation revealed that the method of crosslinking did not bring about major changes to the binding constant (10^{12} M^{-1}) of BSA to nanostructures. Electrostatic binding indicated a larger number of binding sites (2.56) on the protein. Nanoparticle binding brought about a reduction in the characteristic negative ellipticity of BSA, indicating a change in the helical content. The reduction in the elliptical path of BSA was influenced by both nanoparticle curvature and crosslinker, such as in the case of glutaraldehyde or by the nanoparticle curvature alone as in the case of zero length crosslinker – EDC–NHS. Though not a subject matter of this study, the results obtained in this study could have implications in the design of nanobiomaterials, biosafety concerns and their cellular responses.

1. Introduction

One of the fundamental requirements in the development of bio-conjugated materials for imaging, diagnosis and therapeutics is the understanding of how various elements present in the conjugate interact with each other.[1,2] Nanoparticle (NP)–protein conjugates are becoming interestingly relevant for bio-applications. Properties such as binding constants of protein to nanoparticles, protein conformation changes if any, kinetics of binding and morphological changes to the conjugate on binding have been studied through a wide variety of microscopic and spectroscopic techniques.[3]

Gold nanoparticles which show spectroscopic properties,[4–8] that can be modulated by size and shape variations are ideal model nanoparticles for such studies.[9] Capping of the nanoparticles for preventing aggregation can also be modified to incorporate functional molecules that can provide for biological interactions and coupling.[10] Nanoparticle–protein interaction studies have included the role of capping agents such as glutamic acid and citrate on the nanoparticle–protein complexes.[8]

A critical aspect for consideration during nanoparticle functionalisation that has emanated from such studies is the choice of biocompatible coatings. The coating can be either *in situ* or post-synthesis. Of these, nanostructures coated with silica are widely studied – properties of biocompatibility, controllable porosity,[11,12] ability of terminal silanol group to react with various coupling agents, which can covalently attach specific receptor binding peptides to the surface of the nanoparticles among others.[13]

Bovine serum albumin (BSA) is one of the most widely chosen protein for such investigations as it possesses specific fluorescence properties, associated with the two tryptophan residues present on the surface and the hydrophobic pocket.[14] Complexation of the capped or functionalised nanoparticles to the protein can be either covalent or non-covalent. Non-covalent interactions or electrostatic interactions are highly modular in character, such as the case of DNA to nanoparticles. Covalent binding can occur through chemisorptions or bifunctional crosslinkers. Cysteine residues on protein surface or thiol caps on nanoparticles can bring about chemisorption of protein on nanoparticle surface. Bifunctional linkers include aldehydes, carbodiimides and polymers.[15–21]

Several different and separate studies have been carried out to understand the gold nanoparticle/nanoparticle–BSA interactions,[6,22–26] wherein the complexes are formed either through covalent or electrostatic interactions. However, a detailed and

[a]*Laboratory of Bioorganic Chemistry, Department of Biotechnology, Indian Institute of Technology Madras, Chennai – 600036, India. E-mail: anjuc@iitm.ac.in; shobulu@gmail.com*

[b]*National Center for Catalysis Research, Indian Institute of Technology Madras, Chennai – 600036, India*

systematic study on the effect of coating and functionalization of the nanoparticle on protein binding and the conformational changes in the protein following interaction with the functionalized nanoparticle is not reported.

In this work, with the help of numerous experiments, the effect of aminosilane functionalization of gold nanoparticles and their subsequent binding to a model protein–BSA through (a) EDC–NHS (further denoted as Au@Si@NH$_2$^{edc}), (b) glutaraldehyde (further denoted as Au@Si@NH$_2$^{glu}) and (c) direct non-covalent binding through electrostatic interactions between positively charged functionalized Au and negatively charged BSA (denoted as Au@Si@NH$_2$^{ele}) is presented. These studies will serve as a template for obtaining an optimal strategy for design of molecular probes.

2. Materials and methods

2.1 Materials

The glassware used for the present study were pre-treated with aqua regia (3 : 1 v/v ratio of HCl to HNO$_3$) and rinsed thoroughly with Milli-Q water prior to use. Gold chloride and tetraethyl orthosilicate (TEOS) was obtained from Sigma-Aldrich, (3-aminopropyl)triethoxysilane (APTES) and N-hydroxy succinimide (NHS) from Spectrochem Pvt Ltd., India, glutaraldehyde 25% from Merck India and 1-ethyl-3-(3-dimethylaminopropyl) carbodiimide) (EDC) from Acros Organics. All chemicals employed were used as received. Milli-Q water was used for the preparation of all solutions.

2.2 Synthesis of gold nanoparticles

Gold nanoparticles (GNP) with a uniform size of ~20 nm were synthesized using the traditional method of citrate based reduction of gold chloride to gold.[27] Briefly, to 50 mL (1 mM) of HAuCl$_4$ boiling aqueous solution, 5 mL of 38.8 mM of sodium citrate was added rapidly and stirred vigorously under boiling conditions for 15 min and cooled at room temperature.

2.3 Silica coating to gold nanoparticles (Au@Si and surface functionalized with amine group)

GNPs were coated with silica adopting earlier procedures[28–30] with slight modifications. Au@Si was functionalized with amine group according to the procedure described by Liu and Han[29] with slight modification (ESI†).

2.4 Bioconjugation of Au@Si@NH$_2$ to BSA

Direct adsorption of BSA to Au@Si@NH$_2$. Protein can be adsorbed or bound to nanoparticle surfaces through either simple incubation or mixing of the protein and nanoparticle solutions.[31] The stock solution of BSA employed for this study had a concentration of 1 mg mL^{-1}. PBS buffer adjusted to pH 7.4 was employed for preparation of stock and diluents. Au@Si@NH$_2$ prepared by the four methods mentioned above was taken at concentrations ranging from 9.58×10^{-14}–3.01×10^{-10} M with reference to gold nanoparticle concentration and 1 mL of BSA was added. After adding the protein solution to the tubes, the solution was made up to 3 mL with water and the tubes were subjected to vortex for 5 min, following which it was shaken for 30 min. The resultant solution was incubated for five hours for the adsorption/binding of protein to the Au@Si@NH$_2$ to take place. The samples were refrigerated till further experiments.

Covalent conjugation of BSA to Au@Si@NH$_2$. For covalent conjugation of Au@Si@NH$_2$ to BSA via EDC we adopted the method described by Hong et al.,[32] briefly, 1 mg of BSA was dissolved in 10 mL of 50 mM, pH 7.4 PBS buffer. The solution was subjected to vortex for 5 min and to this 1.55 mg EDC and 1.15 mg NHS (N-hydroxysuccinimide) was added, mixed well and allowed to react for one h. One mL of the resultant protein solution was taken in different tubes (the protein concentration was maintained same in all the tubes) and increasing concentrations of Au@Si@NH$_2$ (2.1×10^{-12}–2.1×10^{-11} M) was added to the tubes and made up to 5 mL, mixed well for 3 h and refrigerated.

In another experiment Au@Si@NH$_2$ was covalently bound to BSA using glutaraldehyde as a linker.[33] Briefly, 10 mg of Au@Si@NH$_2$ was taken and 5 mL of 10 mM PBS was added to it. The resultant solution was sonicated for 15 min and to this 1.5 mL of 25% glutaraldehyde was added and shaken for 3 h. The solution was centrifuged at 3500 rpm and redispersed in 5 mL of the buffer. Au@Si@NH$_2$ at concentrations ranging from 1.73×10^{-12}–1.73×10^{-11} M was taken in different tubes and to this 1 mL of BSA (0.1 mg mL^{-1}) was added, made up to 5 mL. The solution was mixed well and allowed to react. These samples were used for binding and characterization experiments.

Electrostatic interaction of BSA to Au@Si@NH$_2$. 10 mg of Au@Si@NH$_2$ was taken and added to 5 mL of 10 mM buffer with a pH of 5–5.5 to obtain a net positive charge to the Au@Si@NH$_2$.[34] From this solution, different volumes of Au@Si@NH$_2$ were taken so as to have a concentration of 4.8×10^{-12} to 2.4×10^{-11} M. To the tubes, 1 mL of BSA (0.1 mg mL^{-1}) was added, made up to 5 mL with the buffer and subjected to mild shaking for 30 min at 25 °C and further allowed to react for 5 h. The samples were used for evaluation of binding efficacy and for characterization experiments.

2.5 UV-visible spectroscopy characterization

UV-visible spectra of GNP, Au@Si@NH$_2$, Au@Si@NH$_2$^{edc}, Au@Si@NH$_2$^{glu}, Au@Si@NH$_2$^{ele} before and after binding to BSA were recorded from 650–400 nm in absorption mode using Jasco B530 UV-visible spectrometer. Protein–nanostructure (NS) interactions, induces Plasmonic shifts on the NS, leading to their clustering arising from proximity to other nanoparticles. The magnitude of such particle clustering can be measured in terms of interparticle distance s, given by the equation:

$$\Delta\lambda/\lambda_o = 0.18 \exp\left[-\frac{(s/D)}{0.23}\right] \tag{1}$$

where $\Delta\lambda/\lambda_o$ is the fractional Plasmon shift, s is the distance between the surfaces of the articles, D is the particle diameter, and 0.23 is the decay constant for the universal trend of plot $\Delta\lambda/\lambda_o$ versus s/D reported elsewhere.[3,21]

2.6 Fluorescence quenching measurements

The intrinsic fluorescence of BSA is mostly due to the tryptophan residues, and hence the emission spectrum of the conjugated samples was run from 300–450 nm, with excitation at 290 nm. A Jasco FP6500 spectroflurometer was employed for the measurements. From the fluorescence spectra, the binding constant (K_b) and the numbers of binding sites (n) between Au@Si@NH$_2$, Au@Si@NH$_2^{edc}$, Au@Si@NH$_2^{glu}$, Au@Si@NH$_2^{ele}$ and BSA can be determined using reported procedure.[22] The details are presented in ESI.†

2.7 Size, size distribution and stability

A Zetasizer 3000HSA (Malvern Instruments, UK), which measures both particle size and zeta (ζ) potential using dynamic light scattering and Doppler electrophoresis was employed for this study. In the particle size mode, each measurement was composed of 10 runs. Intensity average diameter and size distribution was obtained using the inbuilt CONTIN software. For zeta potential values, average of 5 independent measurements were taken. The zeta potential measurements were carried out for Au@Si@NH$_2^{edc}$–BSA, Au@Si@NH$_2^{glu}$–BSA and Au@Si@NH$_2^{ele}$–BSA, with increasing concentration of nanostructure at constant protein concentration.

2.8 Characterization of GNPS, Au@Si, Au@Si@NH$_2$ and Au@Si@NH$_2^{edc}$–BSA, Au@Si@NH$_2^{glu}$–BSA and Au@Si@NH$_2^{ele}$–BSA

The diameter and morphology of GNPs and Au@Si, were investigated using Philips CM12 transmission electron microscope, operating at 120 kV. Energy Dispersive Spectroscopy (EDS) was performed using Au drop coated carbon film on a TEM instrument equipped with EDS attachment. Briefly, a drop of the sample was placed on carbon-coated grids, allowed to dry for 5 min at room temperature. Fourier transform infrared (FTIR) measurements were recorded in transmission mode (600–4000 cm^{-1}) for the understanding of introduction of functional groups on gold nanostructures. The Raman spectra (for BSA, Au@Si@NH$_2^{edc}$–BSA, Au@Si@NH$_2^{glu}$–BSA and Au@Si@NH$_2^{ele}$–BSA) were recorded using a Bruker RFS 27: Standalone FT-Raman Spectrometer model with a laser source iNd: YAG 1064 nm. The power used was 100 mW (srl = 518) with a scan range of 50–4000 cm^{-1} and a resolution of 2 cm^{-1}.

2.9 Circular dichroism (CD) measurements

CD measurements were recorded at 25 °C on a Jasco 715 Circular Dichroism spectropolarimeter. The spectra was measured for every 0.2 nm with a 1 nm band width and at a run speed of 100 nm min^{-1} in the far UV region of 197–250 nm and each spectrum was the average of three scans. The results were expressed as mean residue ellipticity (MRE) in deg cm^2 dmol^{-1}. The concentration of BSA in the CD study was 3.03×10^{-7} M, and the concentration of Au@Si@NH$_2$ in the bioconjugates was 28.8×10^{-12} M.

3. Results and discussion

3.1 Characteristic features of the gold nanoparticles

In this work, the classical citrate reduction method was used to quickly reduce Au(III) to Au(0) which is indicated by the red color produced.[29] From the UV-vis absorbance spectra (Fig. 1), it was observed that the surface plasmon resonance band (SPR) of 510–550 nm occurred at 523 nm, within the reported range.[35] GNPs synthesized (intensity average diameter 27.7 ± 2.1 nm as observed from DLS) were subsequently coated with silica and functionalized with an amine group,[29,30] so as to enable the conjugation with BSA via EDC and glutaraldehyde.

3.2 Morphological features-TEM and DLS analysis

A spherical geometry with diameter ranging from 15–28 nm was observed from TEM of GNPs (Fig. 2A). The electron diffraction pattern recorded for the nanoparticles (inset of Fig. 2A) matched with that of standard gold nanoparticles.[36] Further confirmation to the presence of Au was obtained from energy dispersive X-ray analysis (EDAX) performed after suitable corrections which showed the presence of gold atom (ESI, Table S1†). Information on size was obtained from dynamic light scattering [DLS] technique, where nanoparticles were found to be distributed over a range of 16.7 to 41.8 nm, with hydrodynamic diameter of 27.7 ± 2.1 nm (ESI, Table S2†). The plot of particle size distribution is presented in Fig. S1.†

3.3 IR studies of silica coated GNP

The citrate reduction method follows a two-step reaction with formation of Au–citrate complex as the first step and subsequent reduction of Au and oxidation of citrate as the second.[37] IR spectra of the Au–citrate complex indicated that bands assigned to OH stretching (3495 and 3292 cm^{-1}), C–O stretching of COOH (1754 cm^{-1}) and asymmetric COO– stretching (1712 cm^{-1})[38] were either broadened (3306–3564 cm^{-1}) or
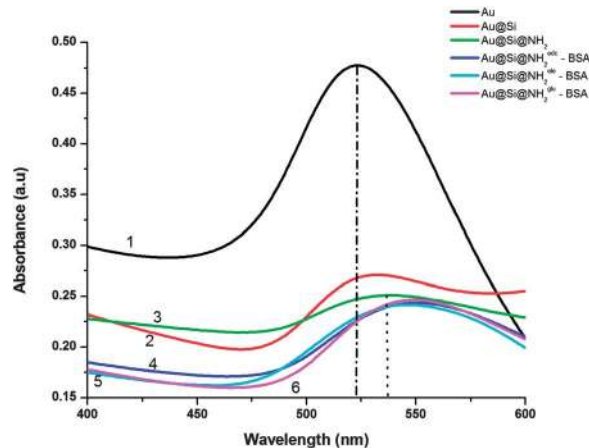

Fig. 1 UV-vis spectra of gold nanoparticles (Au) (1), surface capped nanoparticles (Au@Si) (2) amine coated silica (Au@Si@NH$_2$) (3), BSA linked nanostructures (Au@Si@NH$_2^{edc}$) (4), (Au@Si@NH$_2^{ele}$) (5) and (Au@Si@NH$_2^{glu}$) (6). Dotted lines represent λ_{max} for Au and Au@Si@NH$_2$ at 523 and 537 nm respectively.
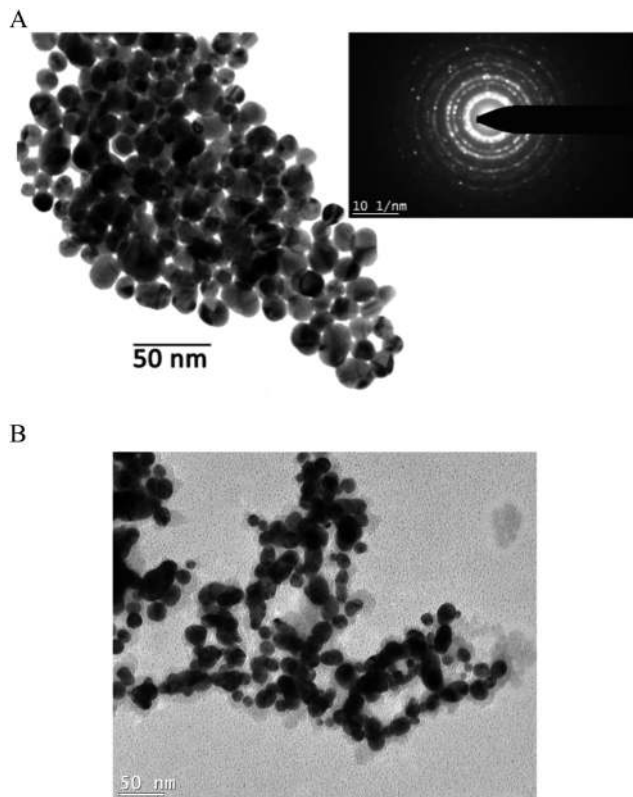
Fig. 2 (A) TEM micrograph of gold nanoparticle and the inset shows the SAED (selected area electron diffraction) pattern of gold nanoparticles. (B) TEM micrograph of silica gold nanoparticle (Au@Si).

Fig. 3 FTIR spectra of gold and gold capped nanostructures (Au, Au@Si and Au@Si@NH₂).

diminished (Fig. 3). The shoulder bands associated with O–H stretching of H-bonded COOH of citrate at 2643 and 2670 cm^{-1} disappeared for the Au(III)–citrate complex, which suggested a competitive binding between H$^+$ and Au(III) for the COO$^-$ in the citrate. The band at 1635 cm^{-1} could be attributed to the reaction product of OH$^-$, H$_2$O and oxidized products of citrate formed during the citrate reduction of Au^{3+} (Fig. 3).[38]

3.4 Characteristic features of the functionalized gold nanoparticles

The SPR of GNPs coated with silica (Au@Si) and subsequently functionalized with amine group (Au@Si@NH$_2$) showed a red shift. For the optimized method of coating, the SPR band was red shifted to 533 nm and 537 nm in the case of Au@Si and Au@Si@NH$_2$ (Fig. 1) respectively. A broadening of the SPR band observed in this study is due to increased scattering of light from the silica.[39]

From the DLS measurements, the hydrodynamic diameter of Au@Si and Au@Si@NH$_2$ was found to be 82 nm and 97 nm (ESI, Table S2†) respectively which explains the red shift in the SPR, as well as the change in the color of the solution from wine red to blue. Contrast variation between the nanoparticles and their surroundings observed in the TEM image of the Au@Si nanostructures (Fig. 2b), confirms the Si coating over Au nanoparticles. The highly reactive Si surfaces provided a sequential connectivity between nanostructures, resulting in the formation
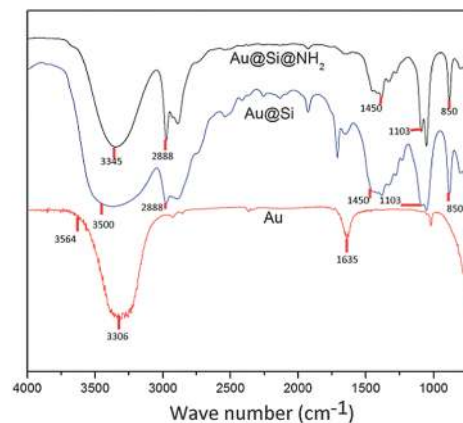
clusters, whose stability in pH 7.4 was reduced as seen from zeta potential values discussed subsequently in this paper similar to previous observations.[39] EDAX analysis (ESI, Table S1†) confirmed the presence of silica in the low contrast regions observed in the micrograph. FTIR spectra (Fig. 3) of Au@Si and Au@Si@NH$_2$ showed bands at 1103 cm^{-1} and 850 cm^{-1}, which can be assigned to the asymmetric and symmetric stretch of the Si–O–Si bond. In the case of Au@Si@NH$_2$, a band observed at 3345 cm^{-1} can be assigned to –NH bond as against the broad band assigned for –OH for Au@Si at 3500 cm^{-1}. In both the cases, –CH$_2$ bending band appears at approximately 1450 cm^{-1} and the –CH stretch band appears at 2888 cm^{-1}.

3.5 Protein nanoparticle assembly

In order to understand the mode of binding of the protein to the functionalized nanostructures, nanostructures were transferred to PBS buffer. A pH of 5.5 was maintained for studying binding through electrostatic interactions, while pH 7.4 was employed for crosslinking through EDC or glutaraldehyde (Scheme 1). Electrostatic interactions cannot be ruled out in the case of EDC and glutaraldehyde mediated interactions, but covalent interactions are dominant. SPR of gold nanoparticles is very sensitive to the surrounding environment such as solvent and mode of binding among others[40] and is known to cause red shifts. However, no such obvious shift in the UV-vis spectra was observed of the nanostructures transferred to PBS buffer at pH 5.5 or 7.4 in this study (data not represented).

On conjugation to BSA, a red shift in the SPR band of Au@Si@NH$_2$ was observed (537 nm → 545$_{ele}$, 549$_{glu}$ and 553$_{edc}$). Interparticle distances between gold nanostructures conjugated to a protein can be directly related to the nanoparticle surface chemistry, density of protein at nanoparticle surface and position of binding site in the protein.[41] By employing λ value of 537 nm for Au@Si@NH$_2$, and an averaged value of three measurements for various conjugated systems, the interparticle distance was calculated using the concept and equation derived by Jain et al.,[42] the determination of interparticle distance between nanostructures conjugated to BSA,
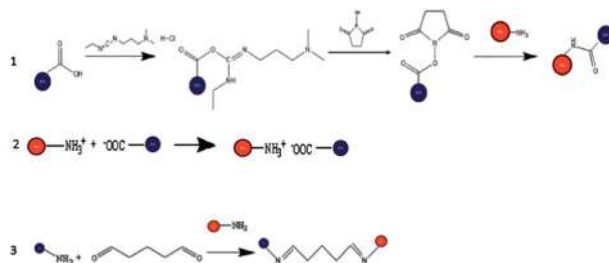
Scheme 1 Scheme reaction of BSA binding to the amine functional-ized nanostructures (Au@Si@NH$_2$). 1 represents covalent binding of BSA to amine functionalized nanostructures *via*, EDC–NHS, 2 repre-sents electrostatic interaction of BSA and amine functionalized nanostructure and 3 represents covalent binding of BSA to amine functionalized nanostructure *via*, glutaraldehyde.

through a particular crosslinking method, provides a direct evidence of the role of a crosslinker in bringing about changes to the structure and morphology of the protein–nanoparticle complex.

Interparticle distance between nanostructures was found to follow the order Au@Si@NH$_2^{ele}$–BSA (65.07 $\pm$ 2.82 nm) > Au@Si@NH$_2^{glu}$–BSA (54.72 $\pm$ 3.51 nm) > Au@Si@NH$_2^{edc}$–BSA (48.66 $\pm$ 3.64 nm). Electrostatic interactions between protein and the functionalized nanostructures is expected to be accompanied by repulsion between two similar charges such as between nanoparticles. The nanostructure–protein system, under such circumstances can be considered to be one at equilibrium, where the forces of repulsion and attraction are matched, resulting in higher separation between two conju-gated nanoparticles. The advantage of zero-length crosslinker can be easily recognized from the interparticle distance. The higher value for the glutaraldehyde mediated system can be attributed to the crosslinker length and possible steric hindrance. In EDC–NHS conjugation of BSA to Au@Si@NH$_2$ the interparticle distance is less. EDC is used for covalent bond formation by activating the COOH group of BSA, which in turn is attracted towards the amine group of the nano-structure resulting in a covalent linkage of nanoparticle and the protein.

3.6 Molecular groups involved in BSA–nanostructure interaction: Raman spectroscopy

Raman spectroscopy was employed in this study to identify the specific molecular groups involved in BSA–nanostructure interaction (Fig. 4). Raman spectra of BSA and its conjugate with gold nanostructures is shown in Fig. 4A. BSA has 583 amino acids and thus 582 peptidic groups corresponding to a molec-ular weight of 66 463 Da.[43] The two tryptophan residues of BSA are characteristically positioned at the surface and hydrophobic pockets at positions 134 and 212, with the one at 134 position being on the surface.[14] Raman shift upon conjugation to the nanostructures through the crosslinkers has been evaluated and is presented in Fig. 4B. The shift in the spectra illustrates the binding and conjugation of nanostructures to the protein. In the case of BSA–Au@Si@NH$_2^{ele}$ and BSA–AU@Si@NH$_2^{edc}$,
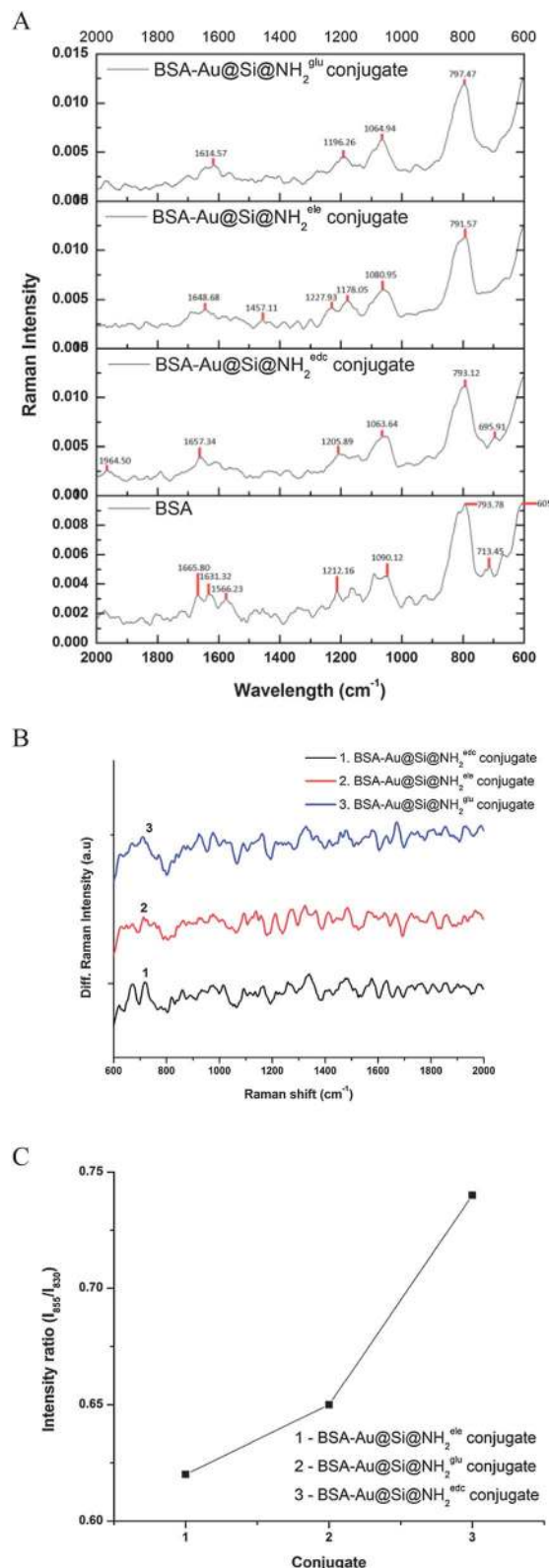

Fig. 4 (A) Raman spectra of BSA and the conjugated BSA. (B) Raman spectral difference of BSA with respect to the BSA linked nano-structure. (C) Intensity ratio (I_{855}/I_{830}) of BSA and conjugated BSA.

the shift in the Raman spectra is attributed to amide I and amide II regions in the crosslinking process, more so in the α helical region of the protein. Conjugation of Au@Si@NH$_2$ through glutaraldehyde to BSA was accompanied by a reduced intensity of the indicated signal at 1614.57 cm^{-1}, suggesting an alteration in α helical content of the protein. Prominent signals at 1227.93 and 1457.11 cm^{-1} in the case of electrostatic interactions, suggest the increasing contribution of β sheets in the binding. Some of the specific bands associated with amino acids in BSA underwent changes on conjugation with nanostructures, indicating their participation in the binding. For instance, tryptophan in the hydrophobic pocket of BSA was involved in binding to the nanostructures, as evidenced from the change in the intensity of the tryptophan band at 1011.28 cm^{-1} (0.00275, 0.00294, 0.00345 and 0.00319 for BSA, BSA–Au@Si@NH$_2$^{edc}, BSA–Au@Si@NH$_2$^{ele} and BSA–Au@Si@NH$_2$^{glu} respectively). Such a binding is reported to decrease the hydrophobicity through an increased net charge on the protein.[44,45] The Fermi resonance (I_{855}/I_{830}) of Tyr residue for the conjugates of BSA with Au@Si@NH$_2$^{edc}, Au@Si@NH$_2$^{glu} and Au@Si@NH$_2$^{ele} (Fig. 4C) was found to be 0.74, 0.65 and 0.63 respectively. A value of less than 1 for the Fermi resonance of Tyr residue, suggests the involvement of phenolic oxygen of tyrosine in BSA in proton donation, leading to a stronger H-bond, more so in the case of BSA–Au@Si@NH$_2$^{ele}.

3.7 Conjugation/absorption – induced BSA conformational changes: circular dichroism

In situ or *ex situ* strategies employed for nanoparticle–protein conjugation need to be evaluated for changes in protein conformation at the interface between nanostructures and protein, *i.e.* the protein in immediate contact with the nanostructures. An extensive review by Mahmoudi *et al.*,[46] looks at the role played by the NP on the thermodynamics and kinetic aspects of NP–protein corona formation. However, the role of the crosslinker on the conformation of protein needs to be addressed A change in protein conformation is likely to lead to changes in functionality of the protein by nanoparticle,[47] such as aggregation and inappropriate interaction with cellular components which leads to cell death. Circular dichroism is the most ideal analytical tool to study the interaction of proteins with other molecules and to understand the conformation of protein is. In this work, the crucial role played by nanoparticle capping and functionalization agent on the protein conformation was evaluated using circular dichroism and fluorescence spectroscopy. Conventional first principle based approaches were employed to quantify the observations.[3,46,48]

BSA has a high percentage of α-helical (67%) structure, which shows a characteristic CD signal in the far UV-region. Changes in the ellipticity at 208 nm and 222 nm are useful probes for understanding changes in the α-helical content of the protein. Fig. 5 shows the typical CD spectra of BSA and BSA conjugated with Au@Si@NH$_2$ through different conjugation methods chosen in this work. CD spectrum of BSA was characterized by a high negative ellipticity due to its rich α-helical content. Conjugation with Au@Si@NH$_2$, indicated a loss of α-

helical content. It is reported that such changes are predominantly at the boundary surface of nanoparticles.[7,49,50] A reduction in negative ellipticity, which followed the order glu > ele > edc is an indication of the extent of perturbation brought about by the crosslinker on the protein. In this work, though a direct measure of the quantum of protein at the protein–nanostructure interface was not available, zeta potential measurements, [discussed in the later part of the study] are indicative of the free protein surrounding the nanostructures. The changes in the helical content of the protein on interaction with the nanostructure has to be related to both, a stronger structural change brought about by the crosslinker or a low degree of surface coverage of the nanoparticle by the protein, as nanostructures induced protein conformation change is also related to the NP curvature.[3] Lesser degree of change to the ellipticity observed when crosslinked through EDC can then be attributed to only surface coating on NP as seen in the case of EDC–NHS.[17,51–53] It is quite possible that the observed changes in helicity of BSA could bring about alterations in protein activity,[54,55] as indicated by a broadening/shift in the Tryptophan fluorescence peak.[56]

3.8 Kinetics of BSA–NS binding: fluorescence spectroscopy

It is well known that presence of Trp, Tyr and Phe residues on BSA contribute to the fluorescence emission from the protein, with Tryptophan having the highest emission intensity due to relatively large excited-state dipole moment.[9] Alongside conformational changes to BSA, the microenvironment around Tryptophan residues in the hydrophobic pocket of domain II and surface of domain I also changes. To understand the kinetics of binding of Au@Si@NH$_2$ in the absence of various crosslinkers to BSA, Tryptophan was employed as an intrinsic probe (λ_{ext} – 290 nm). A decrease in fluorescence intensity of BSA with increasing concentration of Au@Si@NH$_2$ (Fig. 6) was observed, indicating its role in the quenching process. When binding of Au@Si@NH$_2$ occurs at a site in the proximity of any one of the Tryptophan, fluorescence from that Tryptophan would be quenched and the emission would be from the other Tryptophan residue, which is free. Au@Si@NH$_2$ prepared by all the methods in this study [described in ESI†] showed a decrease
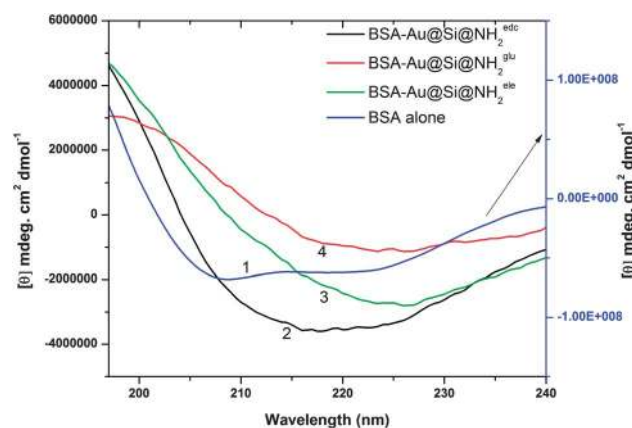

Fig. 5 CD Spectra of BSA and conjugated BSA.

in fluorescence, coupled with a red shift in the emission band of Tryptophan by only about 4 nm, indicating that the changes to the ellipticity of the protein as observed in CD was not significant enough to bring about protein denaturation.

A variation in binding constant and number of binding sites (n) was noticed (ESI†), which indicates polarity changes around tryptophan residues. Changes in the kinetics of binding as brought about by the silica coated nanoparticles, is an indication of the role of protein coating on the nanostructures in bringing about conformational changes to the protein (Fig. S2†).[31] For studies on understanding the role of cross-linkers, an optimized method of synthesis of Au@Si@NH₂ was evolved based on methods which provided for higher binding constant and larger number of binding sites. Binding constants and number of binding sites determined from experiments performed in triplicates and employing Stern–Volmer plots is presented in Table 1. Irrespective of the crosslinker, constant binding values of the order of 10^{12} M^{-1} weres indicative of a strong quenching of the fluorescence of BSA by Au@Si@NH₂ (Fig. 6A–C). This was influenced by the crosslinker as well as the changes that it brings about to the environment around the Tryptophan residue. Interestingly the binding constant obtained in this study was an order of magnitude higher than that reported by Iosin *et al.*, on GNP–BSA conjugates.[9] The method of crosslinking, whether it be through electrostatic interaction or through a zero length or heterobifunctional linker, has no direct role on the kinetics of Au nanostructure-BSA binding. The ability of the crosslinker in bringing about changes to the protein–Au interface, leading to the manner in which the protein is coated over the nanostructure surface thus seems critical. The number of binding sites (n) determined from the intrinsic fluorescence of the protein was found to be higher with non-specific electrostatic interaction as against the covalent interaction. This is expected as EDC–NHS as well as glutaraldehyde crosslinking would occur through specific sites in the protein, the number and accessibility of which controls the binding efficacy.

Table 1 Binding constant and number of binding sites for binding of Au@Si@NH₂ in the presence and absence of cross linkers[a]

Method of conjugation	K_{b} (M^{-1})	n	R
Electrostatic	$0.06 \pm 0.001 \times 10^{12}$	2.56 ± 0.40	0.91 ± 0.07
Glutaraldehyde	$0.19 \pm 0.001 \times 10^{12}$	1.24 ± 0.23	0.89 ± 0.12
EDC–NHS	$0.10 \pm 0.006 \times 10^{12}$	1.50 ± 0.40	0.75 ± 0.11

[a] Values are an average of triplicate measurements.

The results obtained in this study like those reported earlier as[7,57] point to the fact that at a higher ionic strength, the electrostatically driven processes are likely to be perturbed, leaving the covalent interactions intact. In a similar manner, the size and shape of the nanoparticle could influence the interparticle distances and thus the kinetics of binding. Interestingly the shape of the particle also has a role in protecting the protein from heat induced conformational changes.[58]
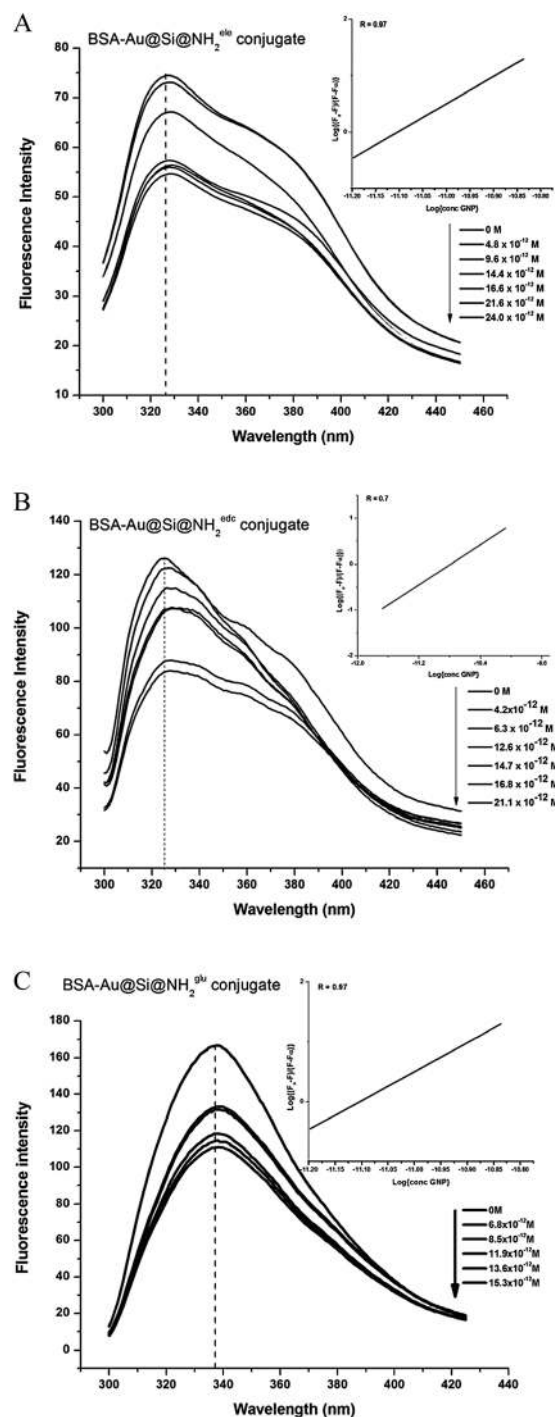

Fig. 6 (A) Fluorescence spectra of BSA and BSA conjugated nanoparticle *via* electrostatic interaction obtained using various concentrations of Au@Si@NH₂. (B) Fluorescence spectra of BSA and BSA conjugated nanostructure *via* EDC–NHS chemistry obtained using various concentrations of Au@Si@NH₂. (C) Fluorescence spectra of BSA and BSA conjugated nanostructure *via* glutaraldehyde crosslinking obtained using various concentrations of Au@Si@NH₂.

3.9 Stability of BSA–NS conjugates: zeta potential measurements

While citrate stabilized gold nanoparticles were very stable (ζ potential -42.8 ± 1.8 mV), silica capping induced an

Table 2 Zeta potential values various BSA–Au conjugated complexes[a]

Conc. of Au@Si@NH$_2$ (M)	Zeta potential (mV)		
	BSA–Au@Si@NH$_2$[ele]	BSA–Au@Si@NH$_2$[edc]	BSA–Au@Si@NH$_2$[glu]
4.8×10^{-12}	-26.3 ± 12.3	-14.9 ± 13.1	-23.8 ± 9.72
24.0×10^{-12}	-24.9 ± 15.7	-16.4 ± 12.2	-31.0 ± 10.2
28.8×10^{-12}	-24.6 ± 17.6	-20.3 ± 12.4	-32.8 ± 9.11
48.0×10^{-12}	-23.1 ± 15.5	-20.5 ± 11.1	-35.4 ± 19.4
52.8×10^{-12}	-22.4 ± 11.3	-20.1 ± 11.3	-34.1 ± 9.06
57.6×10^{-12}	-18.4 ± 19.3	-30.0 ± 8.92	-36.3 ± 8.27

[a] The concentration of BSA used for this study is 3.03×10^{-7} M. The average ζ-potential is on the basis of five measurements.

aggregation of the nanoparticles, as observed from TEM images, with end result of reduction in ζ potential by approximately 10 units (-32 ± 1.4 mV). Amine functionalization further reduced the ζ potential value to -23.8 ± 1.2 mV (measurements being carried out at pH 7.4). The resulting BSA–Au@Si@NH$_2$ complexes prepared as per pH conditions mentioned in Scheme 1 were stable in aqueous media as determined by the zeta potential measurements. BSA imparts stability to networked structure of nanoparticles against aggregation by both electrostatic forces and steric interactions arising from macro proteins siting on adjacent nanostructures preventing the nanostructures from getting closer and aggregating. As expected the net negative charge increases as nanoparticle concentration increases (Table 2) in the case of covalent binding (from -14.9 mV to -36.3 mV). An interesting observation made in this study is that in spite of the Au@Si@NH$_2$[ele] nanostructures being positively charged at pH 5.5, the resulting complex was negatively charged, even at the highest concentration of nanoparticles investigated in this study (from -26.3 mV to -18.4 mV). This observation is an indication of the presence of free BSA surrounding the BSA–Au@Si@NH$_2$ interface, indicated as soft corona elsewhere.[46] It was observed that the percentage of free BSA associated with the protein–nanostructure network follows the order Au@Si@NH$_2$[ele]–BSA > Au@Si@NH$_2$[glu]–BSA > Au@Si@NH$_2$[edc]–BSA (ESI†). The interaction of negatively charged BSA (isoelectric point of BSA – 4.7) with Au@Si@NH$_2$[edc/glu], as expected increases the stability of the resultant complex, as concentration of Au increases. It can be postulated that the covalent binding of the protein to the nanoparticle surfaces, through specific sites on the protein results in a complex with a relatively higher level of stability through a stable balance of attractive and repulsive forces.

4.   Conclusions

In conclusion, the role of mode of binding on the dynamics and mechanism of binding of silica coated Au nanostructures to a model protein BSA has been investigated in detail. Contrary to expectations, the binding constant values for electrostatic and covalent binding of Au nanostructures to protein were similar, while the number of binding sites was higher with non-specific interactions. From the Raman spectra, the possible role of tryptophan in the hydrophobic pocket of the protein in binding to the silica coated nanostructures was identified. The changes in the α-helical content of the protein in immediate contact with the nanoparticle were established using CD spectroscopy. Though both EDC–NHS and glutaraldehyde were involved in covalent crosslinking of Au nanostructures to BSA, the changes in the protein ellipticity was lowest with EDC–NHS conjugation, possibly because change was influenced only by the silica coated and amine functionalized nanoparticle curvature and not by the binding of the linker to the protein surface. Conformational changes to the protein observed in this study were not significant enough to cause protein denaturation as indicated by a minor shift in the fluorescence peak of tryptophan. In conclusion, this work provides an insight into how conjugated systems, with potential applications based on protein conformation and functionalities, could be designed through modification of conjugation method and/or surface coating.

Acknowledgements

Notes and references

1 N. Sanvicens and M. P. Marco, *Trends Biotechnol.*, 2008, **26**, 425–433.

2 C. C. Berry and A. S. G. Curtis, *J. Phys. D: Appl. Phys.*, 2003, **36**, R198–R206.

3 S. H. D. P. Lacerda, J. J. Park, C. Meuse, D. Pristinski, M. L. Becker, A. Karim and J. F. Douglas, *ACS Nano*, 2010, **4**, 365–379.

4 I. H. El-Sayed, X. H. Huang and M. A. El-Sayed, *Nano Lett.*, 2005, **5**, 829–834.

5 P. Ju, H. Fan, T. Liu, L. Cui, S. Ai and X. Wu, *Biol. Trace Elem. Res.*, 2011, **144**, 1405–1418.

6 B. F. Pan, F. Gao and L. M. Ao, *J. Magn. Magn. Mater.*, 2005, **293**, 252–258.

7 L. Shang, Y. Wang, J. Jiang and S. Dong, *Langmuir*, 2007, **23**, 2714–2721.

8 N. Wangoo, K. K. Bhasin, S. K. Mehta and C. R. Suri, *J. Colloid Interface Sci.*, 2008, **323**, 247–254.

9 M. Iosin, F. Toderas, P. L. Baldeck and S. Astilean, *J. Mol. Struct.*, 2009, **924–926**, 196–200.

10 R. A. Sperling and W. J. Parak, *Philos. Trans. R. Soc., A*, 2010, **368**, 1333–1383.

11 S. Liu and M. Y. Han, *Chem.–Asian J.*, 2010, **5**, 36–45.

12 N. Nitin, L. E. LaConte, O. Zurkiya, X. Hu and G. Bao, *J. Bioinorg. Chem.*, 2004, **9**, 706–712.

13 Y. Lu, Y. D. Yin, B. T. Mayers and Y. N. Xia, *Nano Lett.*, 2002, **2**, 183–186.

14 B. Mishra, A. Barik, K. I. Priyadarsini and H. Mohan, *J. Chem. Sci.*, 2005, **117**, 641–647.

15 M. De, P. S. Ghosh and V. M. Rotello, *Adv. Mater.*, 2008, **20**, 4225–4241.

16 M. A. Bangar, D. J. Shirale, W. Chen, N. V. Myung and A. Mulchandani, *Anal. Chem.*, 2009, **81**, 2168–2175.

17 V. Gubala, X. Le Guevel, R. Nooney, D. E. Williams and B. MacCraith, *Talanta*, 2010, **81**, 1833–1839.

18 M. E. Keegan, J. L. Falcone, T. C. Leung and W. M. Saltzman, *Macromolecules*, 2004, **37**, 9779–9784.

19 H. S. Mansur, A. A. P. Mansur and J. C. Gonzalez, *Polymer*, 2011, **52**, 1045–1054.

20 X. Qian, X.-H. Peng, D. O. Ansari, Q. Yin-Goen, G. Z. Chen, D. M. Shin, L. Yang, A. N. Young, M. D. Wang and S. Nie, *Nat. Biotechnol.*, 2008, **26**, 83–90.

21 C. Weber, S. Reiss and K. Langer, *Int. J. Pharm.*, 2000, **211**, 67–78.

22 S. H. Brewer, W. R. Glomm, M. C. Johnson, M. K. Knag and S. Franzen, *Langmuir*, 2005, **21**, 9303–9307.

23 S. Ge, C. Zhang, Y. Zhu, J. Yu and S. Zhang, *Analyst*, 2010, **135**, 111–115.

24 K. K. Haldar, T. Sen and A. Patra, *J. Phys. Chem. C*, 2010, **114**, 4869–4874.

25 N. Kato and F. Caruso, *J. Phys. Chem. B*, 2005, **109**, 19604–19612.

26 C. H. Yu, A. Al-Saadi, S.-J. Shih, L. Qiu, K. Y. Tam and S. C. Tsang, *J. Phys. Chem. C*, 2008, **113**, 537–543.

27 K. C. Grabar, R. G. Freeman, M. B. Hommer and M. J. Natan, *Anal. Chem.*, 1995, **67**, 735–743.

28 D. Kandpal, S. Kalele and S. K. Kulkarni, *J. Phys.*, 2007, **69**, 277–283.

29 S. H. Liu and M. Y. Han, *Adv. Funct. Mater.*, 2005, **15**, 961–967.

30 C. Wang, Z. Ma, T. Wang and Z. Su, *Adv. Funct. Mater.*, 2006, **16**, 1673–1678.

31 M. Iosin, V. Canpean and S. Astilean, *J. Photochem. Photobiol., A*, 2011, **217**, 395–401.

32 J. Hong, P. Gong, D. Xu, L. Dong and S. Yao, *J. Biotechnol.*, 2007, **128**, 597–605.

33 S. Dreis, F. Rothweiler, M. Michaelis, J. Cinatl Jr, J. Kreuter and K. Langer, *Int. J. Pharm.*, 2007, **341**, 207–214.

34 N. R. Jana, C. Earhart and J. Y. Ying, *Chem. Mater.*, 2007, **19**, 5074–5082.

35 C. Jiang, S. Markutsya and V. V. Tsukruk, *Langmuir*, 2003, **20**, 882–890.

36 G. Jiang, L. Wang and W. Chen, *Mater. Lett.*, 2007, **61**, 278–283.

37 W. Patungwasa and J. H. Hodak, *Mater. Chem. Phys.*, 2008, **108**, 45–54.

38 X. Ou, X. Quan, S. Chen, F. Zhang and Y. Zhao, *J. Photochem. Photobiol., A*, 2008, **197**, 382–388.

39 L. M. Liz-Marzan, M. Giersig and P. Mulvaney, *Langmuir*, 1996, **12**, 4329–4335.

40 K. Saha, S. S. Agasti, C. Kim, X. Li and V. M. Rotello, *Chem. Rev.*, 2012, **112**, 2739–2779.

41 L. Calzolai, F. Franchini, D. Gilliland and F. o. Rossi, *Nano Lett.*, 2010, **10**, 3101–3105.

42 P. K. Jain, W. Huang and M. A. El-Sayed, *Nano Lett.*, 2007, **7**, 2080–2088.

43 S. Gam-Derouich, A. Lamouri, C. Redeuilh, P. Decorse, F. o. Maurel, B. Carbonnier, S. Beyazit, G. Yilmaz, Y. Yagci and M. M. Chehimi, *Langmuir*, 2012, **28**, 8035–8045.

44 G. Das, F. Mecarini, F. Gentile, F. De Angelis, H. G. Mohan Kumar, P. Candeloro, C. Liberale, G. Cuda and E. Di Fabrizio, *Biosens. Bioelectron.*, 2009, **24**, 1693–1699.

45 J. Holm, A. J. Lawaetz and S. I. Hansen, *Biochem. Biophys. Res. Commun.*, 2012, **425**, 19–24.

46 M. Mahmoudi, I. Lynch, M. R. Ejtehadi, M. P. Monopoli, F. B. Bombelli and S. Laurent, *Chem. Rev.*, 2011, **111**, 5610–5637.

47 S. Laera, G. Ceccone, F. Rossi, D. Gilliland, R. Hussain, G. Siligardi and L. Calzolai, *Nano Lett.*, 2011, **11**, 4480–4484.

48 J. M. Slocik, A. O. Govorov and R. R. Naik, *Nano Lett.*, 2011, **11**, 701–705.

49 Y. Xiao, W. Xu, Q. Zhu, B. Yan, D. Yang, J. Yang, X. He, S. Liang and X. Hu, *Carbohydr. Polym.*, 2009, **77**, 612–620.

50 X. Jiang, J. Jiang, Y. Jin, E. Wang and S. Dong, *Biomacromolecules*, 2004, **6**, 46–53.

51 N. Wangoo, C. R. Suri and G. Shekhawat, *Appl. Phys. Lett.*, 2008, **92**, 133104.

52 K. Chen, T. J. Merkel, A. Pandya, M. E. Napier, J. C. Luft, W. Daniel, S. Sheiko and J. M. DeSimone, *Biomacromolecules*, 2012, **13**, 2748–2759.

53 N. N. Mamedova, N. A. Kotov, A. L. Rogach and J. Studer, *Nano Lett.*, 2001, **1**, 281–286.

54 L. Fei and S. Perrett, *Int. J. Mol. Sci.*, 2009, **10**, 646–655.

55 M. Kjaergaard, A. B. Norholm, R. Hendus-Altenburger, S. F. Pedersen, F. M. Poulsen and B. B. Kragelund, *Protein Sci.*, 2010, **19**, 1555–1564.

56 L. Shang, Y. Z. Wang, J. G. Jiang and S. J. Dong, *Langmuir*, 2007, **23**, 2714–2721.

57 A. Verma, J. M. Simard and V. M. Rotello, *Langmuir*, 2004, **20**, 4178–4181.

58 S. Singha, H. Datta and A. K. Dasgupta, *J. Nanosci. Nanotechnol.*, 2010, **10**, 826–832.